Published in final edited form as:
Bioconjug Chem. 2009 November ; 20(11): 2047–2054. doi:10.1021/bc900150v.

Physico-Chemical Characterization of Polylipid Nanoparticles for Gene Delivery to the Liver

Maung T. Nyunt[†], **Christopher W. Dicus**[‡], **Yi-Yao Cui**[§], **M. Cecilia Yappert**[‖], **Thomas R. Huser**[†], **Michael H. Nantz**[‖], and **Jian Wu**[§,*]

[†]NSF Center for Biophotonics Science and Technology, University of California, Davis Medical Center, Sacramento, California 95817

[‡]Department of Chemistry, University of California, Davis, California 95616

[§]Department of Internal Medicine, Transplant Research Program, University of California, Davis Medical Center, Sacramento, California 95817

[‖]Department of Chemistry, University of Louisville, Louisville, Kentucky 40292

Abstract

Polylipid nanoparticles (PLNP) have been shown to be very effective in delivering antioxidative genes in the treatment of liver injury in mice. To build on our previous studies and to further characterize PLNP formulated from polycationic lipid (PCL) and cholesterol, we report here the synthesis of multigram quantities of PCL and employ analytical tools, such as Raman spectroscopy of single PLNP and live-cell imaging of lipofection, for the physicochemical characterization of PCL, PLNP, and the transfection process. Mass spectrometry demonstrates the characteristics of polymeric lipids. Raman spectrum of PCL reveals the polymeric structure of the polymers. The presence of cholesterol in PLNP formulation did not markedly change the Raman spectrum. PLNP-derived polyplexes exhibit Raman spectra very similar to PLNP except that the C–H out-of-plane deformation mode of the polymeric lipid is significantly suppressed, indicating the interaction with plasmid DNA. Zeta potential measurement indicates a large DNA-carrying capacity of PLNP and their stability for *in vivo* gene delivery. The live-cell fluorescent imaging dynamically shows that PLNP exerts transfection efficiency similar to lipofectamine in leading to early reporter gene expression in live hepatic cells. In conclusion, polylipid nanoparticles possess a high DNA carrying capacity and lipofection efficiency, rendering them suitable for testing in large animals. The employment of novel state-of-the-art technologies in the study of lipofection represents the level of physicochemical and biological characterization that is needed to best understand the key elements involved in the lipofection process.

INTRODUCTION

Lipid nanoparticles (LNP) have been used widely for *in vitro* gene delivery; however, their potential for *in vivo* gene delivery has been hampered by stability issues in the bloodstream, poor targeting efficiency, and transient transfection efficacy (1). Polylipid nanoparticles

[*]All correspondence should be addressed to Jian Wu, MD, PhD, Department of Internal Medicine, Transplant Research Program, UC Davis Medical Center, 4635 2nd Ave. Suite 1001, Sacramento, CA 95817, Tel.(916)734-8044, Fax:(916)734-8097, jdwu@ucdavis.edu. Michael H. Nantz, PhD, Department of Chemistry, University of Louisville, Louisville, KY 40292, Tel. (502) 852-8069, Fax: (502) 852-8149, mhnant01@louisville.edu.

Supporting Information Available: The use of the DVDM system enables us to section cells at 0.1 μm thicknesses, and a three-dimensional structure of a cell can be built from the sections at the *Z* axis. This material is available free of charge via the Internet at http://pubs.acs.org.

(PLNP), formulated from polycationic lipid (PCL) and cholesterol, on the other hand, have been documented to be more stable than DOTAP-DOPE1 or DOTAP-cholesterol formulations in the bloodstream (2). We have also shown that PLNP-derived polyplexes were effective in delivering reporter genes, human antioxidative genes (extracellular superoxide dismutase (EC-SOD) or catalase) to the liver for the treatment of acute liver injury caused by hepatotoxins, or an ischemia/reperfusion procedure in two separate preclinical model systems (3, 4). These studies suggest that PLNP are a very effective gene transfer agent for liver-based delivery and have great potential to move from small animals to large animal trials as a step toward clinical applications (5). To develop an even more biocompatible gene delivery agent and to move this antioxidative gene approach from "bench to bedside", in-depth characterization of PCL, PLNP, and polyplexes, as well as feasible technologies for larger-scale synthesis of PCL, are needed. In this study, we employ state-of-the-art technologies, such as Raman microspectroscopy, mass spectrometry, and DeltaVision deconvolution microscopy (DVDM) for live cell imaging together with zeta potential measurements to further characterize PCL, PLNP, and PLNP-derived polyplexes. These novel technologies enable us to characterize the physicochemical features of PCL, PLNP, and PLNP-derived polyplexes, as well as the lipofection process, and further determine the stability of the polyplexes. We also describe modifications to our original method of PCL synthesis that enable multigram preparations of PCL sufficient for large animal experiments.

EXPERIMENTAL PROCEDURES

Synthesis of PCL

Synthetic Procedures and Validation—PCL (**1**) was prepared according to the synthetic route outlined in Figure 1. Prior to use, CH_2Cl_2 was immediately distilled from CaH_2. After reaction workup, solutions were dried using Na_2SO_4, and solvents were subsequently removed by rotary evaporation. Nuclear magnetic resonance (NMR) spectra were recorded with a General Electric QE-300 spectrometer (^1H at 300 MHz, ^{13}C at 75 MHz). Infrared spectra were recorded on a Mattson Genesis II FTIR 3000 spectrometer. Melting points are uncorrected. Elemental analyses were performed by Midwest Microlabs (Indianapolis, IN). All sonications were performed in a bath sonicator (Laboratory Supplies Inc., Hicksville, NY).

3-Bromo-1,2-bis(tetradecanoyloxy)propane (3)—To a solution of 3-bromo-1,2-propane-diol (**2**) (9.20 g, 59.4 mmol) in CH_2Cl_2 (50 mL) were added triethylamine (16.5 mL, 119 mmol) and 4-(*N*,*N*-dimethylamino)pyridine (400 mg). The reaction mixture was cooled to 0 °C, and then myristoyl chloride (40.4 mL, 149 mmol) was added dropwise. The reaction was warmed to room temperature and quenched after 4 h by pouring over saturated aqueous $NaHCO_3$ (100 mL). The aqueous layer was separated and the organic layer was washed successively with saturated aqueous $NaHCO_3$, water, and brine, and then dried (Na_2SO_4). The solvents were concentrated in vacuum, the crude residue was dissolved in ethanol, and minimal water was added to provide a cloudy suspension. The solution was placed in the freezer overnight causing bromodiester **3** to precipitate as a white solid (31.4 g, 54.6 mmol, 92%); mp 40–41.5 °C; IR (neat) 2913, 2848, 1731 cm^{-1}; ^1H NMR ($CDCl_3$) δ 0.85 (t, *J* = 6.6 Hz, 6H), 1.23 (m, 40H), 1.59 (m, 4H), 2.29 (m, 4H), 3.48 (m, 2H), 4.21 (dd, *J* = 11.9, 5.6 Hz, 1H), 4.30 (dd, *J* = 11.9, 4.4 Hz, 1H), 5.18 (m, 1H); ^{13}C NMR ($CDCl_3$) δ

[1]Abbreviations: DOPE, L-α dioleoyl phosphatidylethanolamine; DOTAP, 1,2-bis(dioleoyloxy)-3-(trimethylammonio)propane; LNP, lipid nanoparticle; PCL, poly(cationic lipid); NMR, nuclear magnetic resonance; PLNP, polylipid nanoparticles; DVDM, DeltaVision deconvolution microscope.

14.0, 22.6, 24.8, 29.0–29.8 (6 signals), 31.9, 33.9–34.1 (3 signals), 62.9, 69.9, 172.6, 173.0; Anal. Calcd for $C_{31}H_{59}O_4Br$: C, 64.68; H, 10.33. Found: C, 64.75; H, 10.32.

3-(N-Methyl-N-(2-N′-acrylamide-N′-methylamino)ethyl)amino)-1,2-bis(tetradecanoyl-oxy)propane (4)—To a solution of bromo diester **3** (23.9 g, 42.8 mmol) in *N*,*N*-dimethylformamide (200 mL) was added *N*,*N*′-dimethylethylenediamine (DMF) (36.8 mL, 342 mmol) via a syringe. The reaction was stirred under an argon atmosphere at 70 °C. After stirring 45 min, DMF and the unreacted diamine were removed by vacuum distillation. The residue was suspended in CH_2Cl_2 (250 mL) and washed successively with saturated aqueous $NaHCO_3$, water, and brine, and then dried (Na_2SO_4). The solvent was removed, and the crude product was passed through a short column of silica gel, eluting with 15% MeOH/CH_2Cl_2, to afford the crude diamino diester as yellow oil (9.6 g).

To a solution of the crude diamino diester (9.6 g, 16.5 mmol) in CH_2Cl_2 (100 mL) at 0 °C were added triethylamine (2.3 mL, 16 mmol) and 4-(*N*,*N*-dimethylamino)pyridine (200 mg). Acryloyl chloride (1.6 mL, 25 mmol) was added dropwise to the resulting solution, and the reaction mixture was warmed to room temperature. After stirring 3 h, the reaction was quenched by pouring over saturated aqueous $NaHCO_3$. The layers were separated, and the organic layer was washed with water and brine, dried (Na_2SO_4), and then concentrated by rotary evaporation. The residue was purified by column chromatography (SiO_2), eluting with a 3:2 mixture of EtOAc/hexane, to give the diester acrylamide **4** as a light yellow oil (8.72 g, 13.7 mmol, 32%); IR (neat) 2921 2852, 1737, 1654, 1614 cm^{-1}; ^1H NMR ($CDCl_3$) δ 0.87 (t, *J* = 6.6 Hz, 6H), 1.25 (m, 40H), 1.59 (m, 4H), 2.30 (m, 7H), 2.57 (m, 4H), 3.00 (s, 1.5H)*, 3.09 (s, 1.5H)*, 3.41 (m, 1H)*, 3.50 (m, 1H)*, 4.06 (m, 1H), 4.30 (m, 1H), 5.15 (m, 1H), 5.67 (dd, *J* = 10.2, 2.10 Hz, 1 H), 6.30 (dd, *J* = 2.1, 16.8 Hz, 0.5 H)*, 6.32 (dd, *J* 2.0, 16.7 Hz, 0.5 H)*, 6.60 (dd, *J* = 10.2, 16.8 Hz, 1H); ^{13}C NMR ($CDCl_3$) δ 13.9, 22.5, 24.7, 28.9–29.4 (5 signals), 31.7, 34.0, 34.2, 36.0, 42.7, 43.0, 45.8, 48.2, 55.3, 56.3, 57.6, 58.0, 63.4, 63.6, 69.0, 69.2, 127.4, 127.6, 166.0*, 166.3*, 172.9, 173.1. Anal. Calcd for $C_{38}H_{72}O_5N_2$: C, 71.65; H, 11.39; N 4.40. Found: C, 71.32; H, 11.47; N 4.35. (*signals arising from amide stereoisomers).

***N*-(2-(*N*′-Acryloyl-*N*′-methylamino)ethyl)-*N*,*N*-dimethyl-*N*-[2,3-bis(tetradecanoyloxy)] propanammonium chloride (5)—**Acrylamide **4** (8.68 g, 13.6 mmol) was dissolved in methyl iodide (25 mL) and stirred at room temperature. After stirring for 18 h, methyl iodide was removed using a stream of argon. The crude residue was purified by column chromatography (SiO_2), eluting with a 9:1 mixture of CH_2Cl_2/MeOH. The product then was passed through a column of Dowex 1 × 8–400 ion-exchange resin (~70 g), eluting with MeOH, to give **5** as a white solid (8.63 g, 12.6 mmol, 92%); IR (neat) 3564, 3358, 2954, 2916, 2848, 1743 cm^{-1}; ^1H NMR ($CDCl_3$) δ 0.84 (t, *J* = 6.2 Hz, 6H), 1.22 (m, 40H), 1.54 (m, 4H), 2.28 (m, 4H), 3.27 (s, 3H), 3.38 (s, 3H), 3.41 (s, 3H), 3.88 (m 2H), 4.04 (m, 4H), 4.29 (d, *J* = 13.8 Hz, 1H), 4.47 (dd, *J* = 2.6, 11.6 Hz, 1H), 5.59 (m, 1H), 5.73 (dd, *J* = 1.5, 10.5 Hz, 1H), 6.29 (dd, *J* = 1.5, 16.5 Hz, 1 H), 6.57 (dd, *J* = 10.4, 16.7 Hz, 1H); ^{13}C NMR ($CDCl_3$) δ 13.9, 22.5, 24.6, 24.7, 29.0–29.5 (4 signals), 31.8, 33.8, 34.1, 36.1, 42.3, 51.9, 62.5, 63.3, 64.2, 66.0, 127.2, 128.5, 167.3, 172.5, 172.9.

The Final Product, PCL (1)—Monomer **5** (4.32 g, 6.28 mmol) was suspended in nanopure water (400 mL) by sonication at 50 °C for 45 min. The resultant homogeneous suspension was degassed by bubbling a stream of nitrogen through the suspension for 20 min. The suspension then was heated to 80 °C and stirred vigorously while adding *n*-dodecyl mercaptan (432 mg, 2.13 mmol), followed by a solution of 2,2′-azobis(2-methylpropionamidine) dihydrochloride (AAPH) (175 mg in 45 mL H_2O, 0.645 mmol). The resulting mixture was stirred at 80 °C for 15 h, after which the reaction vessel was placed in

a freezer overnight (−10 °C). After thawing at room temperature, the precipitated solids were filtered and washed successively with cold diethyl ether to remove trace mercaptan and then dried under vacuum to afford PCL (4.21 g, 97%) as a white solid with spectral characterization identical to that previously reported (6).

Mass Spectral Analysis of PCL

PCL (5 mg) was dissolved in 1 mL of isopropanol. Both a 0.17 M solution of *para*-nitroaniline (PNA) and a 0.5 M solution of 2,5-dihydroxybenzoic acid (DHB) were prepared in isopropanol and used as matrices. PNA has been used previously for the detection of phospholipids in positive- and negative-ion spectra (7). A 1 μL aliquot of the analytical solution was spotted in each of five different sample wells of a 100-spot stainless steel MALDI plate (Applied Biosystems, Foster City, CA). The matrix (1 μL) was then added on top of each sample spot (dried droplet method). After crystallization at ambient conditions, mass spectra were recorded on a Voyager Biospectrometry DE workstation (Applied Biosystems, Foster City, CA) equipped with a Nitrogen laser (λ = 337 nm). The extraction voltage was set to 20 kV. Mass spectra were acquired in both positive and negative modes.

Raman Micromicroscopy Analysis of PCL, PLNP, and PLNP-Derived Polyplexes

The Raman spectra of various LNP formulations were acquired using a Laser-Tweezers Raman microspectroscopy system, which is custom-built around a commercial inverted microscope platform (8). The main microscope frame consists of an Olympus IX-71 microscope, utilizing a 60×, NA 1.2, water immersion objective optimized for near-infrared operation. The laser source is an 80 mW, 785 nm diode-pumped solid-state laser, resulting in ~30 mW laser power in the microscope focus after passing multiple mirrors, a bandpass filter, and the microscope objective. The laser beam is focused to a diffraction-limited laser spot of ~500 nm diameter. The microscope is equipped with a mercury arc lamp for white-light fluorescence excitation through appropriate filters, as well as differential interference contrast for visualizing cells. Laser trapping and fluorescence excitation can be performed simultaneously. Spectroscopy is performed through an attached SP2300i spectrograph (Acton Research Corporation) and a back-illuminated thermoelectrically cooled deep-depletion CCD camera with 1340 × 1000 pixels (Figure 2).

The Use of a Fluorescence Deconvolution Microscopy System to Monitor the Lipofection Process

The automated fluorescence deconvolution microscopy system (9) (Personal DV, Applied Precision, LLC., Issaquah, WA) makes use of an Olympus IX-71 inverted optical microscope with a 250 W xenon illumination source, a 60× oil-immersion objective lens with a numerical aperture (NA) of 1.4 and a precision stepper-motor driven XYZ stage. The microscope is equipped with DAPI, FITC, TRITC, CY3, and CY5 filter sets, as well as 5 neutral density filters for the excitation source. It is capable of exciting fluorophores from the UV to the far-red and also collects transmitted light (bright field, differential interference contrast (DIC)) images. Image capture is achieved with a CoolSnap ES2 (Photometrics, Tucson, AZ)—a fast, high-resolution, high quantum efficiency, thermoelectrically cooled CCD camera. It can be used for both slow scan, high-resolution imaging of fixed samples or fast, high-sensitivity image capture of live cell samples.

The DeltaVision acquisition, image processing, and analysis software (*softWoRx 3.7.0*) run on a dual-processor personal computer running Cent OS Linux. The microscope is capable of separating up to 4 dyes and displaying triply labeled samples in a single image window through false colors. The DeltaVision software package automates the deconvolution computations, generates 3D reconstructions, and enables autofocusing, cell tracking, and live-cell imaging.

In our experiment, Hep G_2 cells were seeded on 35-mm-diameter round glass bottom culture dishes (MatTek Corp., Ashland, MA). The next day, cells were transfected with plasmid pEGFP-C1 by either PLNP or Lipofectamine, and then incubated at 37 °C. At specified time points, the culture dishes were mounted on the DeltaVision Deconvolution microscope. The temperature of the microscope stage was kept constant at 37 °C using an air-stream incubator (ASI-400, NevTek, Williamsburg, VA). GFP fluorescence of Hep G_2 cells was detected using a standard FITC filter set and corresponding bright field images were also collected. A series of images at different vertical focus positions resulting in optical sections (step size 0.1 μm) were captured with an image size of 512 by 512 pixels and setting binning to 2 × 2. The exposure time of between 0.1 to 0.3 s was sufficient to obtain images suitable for the dynamic range of the cooled CCD camera. Images were saved and processed using the DeltaVision software package (*softWoRx 3.7.0*) and Adobe Photoshop CS3.

Zeta Potential of PCL, PLNP, and Polyplexes

PLNPs were generated as reported previously and complexed with plasmid DNA at different charge ratios. The size distribution was determined by laser light scattering as reported previously (10). PLNPs or polyplexes in 2 μL were suspended in 2.5 mL water, and their zeta potentials were determined at room temperature in a Zeta Potential/Particle Sizer Nicomp 280 ZCS PSS-Nicomp Particle Sizing System (Santa Barbara, CA).

Statistical Analysis

The data of zeta potential in different charge ratios were analyzed by one-way variance test followed by multiple comparisons between groups with Newman-Keuls test. A *p*-value of less than 0.05 was considered as statistically significant.

RESULTS

Synthesis of PCL in a Multigram Quantity

The PCL synthesis proceeded from commercially available diol **2** by bisesterification using myristoyl chloride. Subsequent bromide displacement by *N*,*N*′-dimethylethylenediamine followed by reaction of the crude adduct with acryloyl chloride gave acrylamide **4**. Amine quaternization followed by counterion exchange using an established procedure (11) afforded acrylamide **5** as the chloride salt. The polymerization of **5** was accomplished by heating a suspension of **5** in water (ca. 15 mM) to 80 °C and then adding *n*-dodecyl mercaptan (12) and the water-soluble free radical initiator 2,2′-azobis(2-methylpropionamidine) dihydrochloride (AAPH) (13). The delay in addition of *n*-dodecyl mercaptan until the formulation of lipid nanoparticle with **5** differs from our previous protocol (6) and helps minimize conjugate addition of the thiol to the acrylamide. All intermediate products were validated by NMR spectral analysis, and the final polymeric product was determined in both negative and positive modes by mass spectral analysis (MALDI-TOF MS). The strongest MALDI-TOF MS signals were obtained with the use of *para*-nitroaniline (PNA) as the matrix. Although no detectable peaks were obtained in the negative mode, strong signals with maximal intensity at m/z = 651.6 were observed in positive-ion spectra, consistent with a polymeric product derived from monomer **5** (Figure 3). The product arising from conjugate addition of dodecyl mercaptan to the acrylamide moiety of **5** was observed at m/z = 853.6. Thus, our modified synthetic method produced PCL in multigram quantities, which is essential for generating enough PLNP for experiments in large animals.

Raman Spectroscopic Analysis of PCL, PLNP, and PLNP-Derived Polyplexes

We have obtained Raman spectra of the various starting materials at high concentration, such as plasmid DNA (3.6 μg/μL), pure lipofectamine, and pure cholesterol as received from the manufacturer, as well as unformulated PCL as synthesized (Figure 4A). For comparison, spectra of lipofectamine complexes with plasmid DNA (Figure 4B), as well as those of PCL vesicles, PLNP, and PLNP-derived polyplexes, were taken (Figure 4C). The Raman data from unformulated PCL are due to Raman scattering on carbon bonds, i.e., C–C, C=C, C–H, CH_2, and clearly show the polymeric nature of PCL (14, 15). The most prominent peaks are C–C stretch modes in the 1100–1200 cm^{-1} and the 1300 cm^{-1} range, and the 1445 cm^{-1} methylene bending vibration in the polymer. Similar features with less pronounced peaks besides the 1445 cm^{-1} methylene deformation mode were found for lipofectamine and cholesterol. Cholesterol contains an additional strong C=C vibration at ~1670 cm^{-1}. The spectrum of plasmid DNA (Figure 4A) is dominated by DNA marker modes such as the 785 cm^{-1} cytosine ring breathing vibration, the 1090 cm^{-1} vibration from the phosphate backbone, the abundant 1442 cm^{-1} CH mode, and the 1575 cm^{-1} adenine vibration (16). In addition, this spectrum contains contributions from the solvent (Tris-EDTA buffer) at 1060 cm^{-1}, as well as from polysaccharides from bacterial lysate at 860 cm^{-1} (15, 17). These endotoxins are, however, only present in this highly concentrated form of plasmid DNA, which was required to obtain its Raman spectrum. The DNA used for forming lipoplexes or polyplexes is free of endotoxins. The spectrum of lipofectamine remains unaltered upon dilution (data not shown). Lipofectamine-derived lipoplexes exhibit combined Raman peaks due to lipofectamine as well as DNA. Most noticeable are a weak 785 cm^{-1} cytosine breathing mode, the 1090 cm^{-1} vibration from the phosphate backbone, and the 1660 cm^{-1} amide I mode (Figure 4B). Raman spectra were acquired from individual optically trapped PCL, PLNPs, and PLNP polyplex vesicles within a 30 s signal integration time. Interestingly, PCL changes its spectrum between unformulated PCL and formulated PCL nanoparticles. Most notable is the addition of a strong 1001 cm^{-1} C–H out-of-plane deformation mode. C–H and C–C modes in this spectral range are known to be sensitive markers of acyl chain disorder (8, 14). This has been widely observed in lipid vesicles. On the basis of these observations, we attribute this strong peak to the increased chain disorder in formulated PCL when compared to unformulated PCL powder. Interestingly, the addition of cholesterol to PCL nanoparticles to form PLNP does not noticeably change the Raman spectrum of these particles, i.e., the disordered state of the polymer chains is retained in the presence of cholesterol. PLNP-derived polyplexes undergo a marked change in their Raman spectrum when compared to PLNP. Here, the 1001 cm^{-1} C–H out-of-plane deformation mode is significantly suppressed due to interaction with plasmid DNA. We attribute this to strong interactions of the charged DNA backbone with the charged polymer chains, which apparently leads to strong ordering in the vesicle chain structure (Figure 4C). The presence of DNA in polyplexes is further confirmed by the presence of weak DNA markers, such as the 785 cm^{-1} cytosine breathing mode, the 1090 cm^{-1} phosphate vibration, and the 1660 cm^{-1} amide I mode.

Use of Fluorescence Deconvolution Microscopy to Dynamically Monitor Reporter Gene Expression

To dynamically determine the earliest expression of a reporter gene, enhanced green fluorescent protein (GFP), we employed a fluorescence microscopy imaging system for time-elapsed live cell imaging to compare the transfection efficiency of PLNP with lipofectamine. As shown in Figure 5, the earliest GFP expression in Hep G_2 cells was seen 60 min after PLNP-mediated transfection with a pEGFP-C1-EGFP plasmid at the charge ratio of 5:1 (Figure 5A,D), while focal and faint GFP expression was also seen in Hep G_2 cells 70 min after lipofectamine transfection (Figure 5G,J), indicating that lipid nanoparticle-mediated plasmid DNA entering a cell and the nucleus, i.e., the transcription of the reporter

gene, is a rather fast process. GFP expression then became more intense and spread throughout Hep G_2 cells transfected either with PLNP (Figure 5B,C,E,F) or lipofectamine (Figure 5H,I,K,L). This observation indicates that the transfection efficiency of PLNP is at least as good as lipofectamine in Hep G_2 cells.

Zeta Potential, Charge Ratios, Size, and Visualization of PLNP and Polyplexes

In order to further determine the relationship of charge ratios and zeta potential of PLNP and PLNP-derived polyplexes, we mixed PLNP with plasmid DNA at various charge ratios, and measured the zeta potential and size of PLNP and PLNP-derived polyplexes at the same time. It is clear from Figure 6 that, for *in vitro* transfection at a charge ratio of 5:1, the zeta potential of polyplexes was slightly lower than PLNP without DNA ($p > 0.05$). For *in vivo* gene delivery at the charge ratio of 1.25:1, the zeta potential of the polyplexes was negative (-6.46 ± 0.97 mV), which is consistent with them being less reactive to serum proteins as reported previously (2). We also noticed that the size of polyplexes increased when PLNP were complexed with plasmid DNA. The polyplex size was within the range 200–400 nm, which are similar to many other lipid formulations reported (18, 19). The stability of our PLNP was further confirmed *in vitro* when PCL and PLNP vesicles were prepared by sonication to result in nanoparticles with a diameter of 149 ± 62 nm. Under the microscope, we were able to visualize the vesicles of both PCL and PLNP by their absorption of transmitted light (highlighted by a circle) (Figure 7A). The vesicles appear homogeneous in size and shape. The morphology of these particles did not change significantly after complexation with plasmid DNA (Figure 7B), whereas lipofectamine formed large aggregates in the presence of plasmid DNA (4 μL liposomes/2 μg DNA) (Figure 7C). These data indicate that our PLNP formulation is superior to lipofectamine in DNA binding capacity and particle stability when forming complexes with plasmid DNA.

DISCUSSION

In our previous study, a cationic acrylamide lipid was polymerized to form PCL (6). Our PLNP formulated from PCL and cholesterol have been considered as one of a few nonviral lipid nanoparticle formulations (20, 21) useful for *in vivo* gene transfer due to their nontoxic feature, high stability in the bloodstream, and superior transfection efficacy in mouse liver (2, 6). The preclinical proof-of-concept experiments in two separate model systems demonstrated that the delivery of antioxidative genes, either EC-SOD or catalase, or in combination, protected mouse from acute liver injury induced by hepatotoxins or hepatic ischemia/reperfusion procedures (3, 4). These studies were highlighted as “the basis for studies with larger animals and may help bridge the gap between the basic understanding of pathophysiologic processes in animal models towards a practical clinical application in liver transplantation” (5). In order to perform large animal experimentation, such as in pigs or nonhuman primates, or for clinical use, we developed a feasible synthetic route for synthesizing PCL on a relatively large scale. The purity of the final product with the polymeric features was verified by mass spectrometry; and PLNP were formulated with the final product and used in the experiments of this study.

Raman spectroscopy is a laser-based analytical technique that enables chemical characterization of molecules in microscopically small samples (8). Raman microspectroscopy is based on the inelastic scattering of photons by molecular bond vibrations and is a useful tool for the chemical analysis of lipids, lipoplexes, or polyplexes due to its ability to provide chemical group identification (22). A particular advantage of micro-Raman spectroscopy is its unrivaled sensitivity and its relative noninvasiveness, which enables the nondestructive analysis of nanoscopic compounds as small as 50 nm diameter (8, 14). We have employed Raman microspectral analysis in a number of studies (23, 24), including analyzing the chemical composition of individual triglyceride-rich

lipoproteins (25). A Raman spectrum appears when a small portion of the photons from a monochromatic light source is scattered by interaction with the bonds resulting in a shift toward higher or lower frequencies. The energy difference between the incident and scattered photons corresponds to the vibrational energy of the specific molecular bond interrogated. A Raman spectrum obtained from lipids, DNA, or their complexes provides an intrinsic molecular fingerprint of these samples, and reveals characteristic information about macromolecular conformations (8). In order to further characterize the chemical features of PCL, PLNP, and PLNP-derived polyplexes, we employed a laser-tweezers Raman microspectroscopy system to observe morphologic changes in these particles after complexation with plasmid DNA and to acquire Raman spectra of polyplexes and compare them with lipofectamine lipoplexes. After carefully comparing with pure reagents for PLNP formulation and polyplex formation, we found that the Raman spectra of PCL exhibits polymeric characteristics of the synthetic polymer and that the spectra of PLNP indicate that they readily interacted with plasmid DNA and formed complexes without aggregation. Lipofectamine, on the other hand, was observed to form large aggregates devoid of specific interactions with DNA after complexation with plasmid DNA. These findings, which have not been reported, imply the feasibility of *in vivo* application of PLNP.

The appearance and extent of reporter gene expression in transfected cells are generally determined either by measuring activity of luciferase after lysing cells or by observing the onset of fluorescence from GFP expression at certain time points with a regular fluorescent microscope. It is generally believed that the lipofection process usually takes at least 6 h in transfected cells (26). In our previous experiments, we compared transfection efficiency in Hep G_2 cells between PLNP and lipofectamine by luciferase activity and cytotoxicity, and found that PLNP is less toxic than lipofectamine in primary hepatocytes and displayed transfection efficiency in Hep G_2 cells similar to lipofectamine (6). The automated fluorescence microscopy imaging system offers the possibility to dynamically monitor the transfection process in live cells, and we noticed that the earliest GFP appearance was within 1 h in Hep G_2 cells transfected with PLNP, and a relatively faint GFP image was also seen in Hep G_2 cells transfected with lipofectamine 20 min later. Thereafter, the intensity and spread of GFP were similar in cells transfected by either PLNP or lipofectamine. Thus, we were able to dynamically monitor an early lipofection process in live cells over time. The time-lapsed imaging mode of the automated fluorescence deconvolution microscope minimizes long-term photobleaching by rapidly shuttering the excitation source on and off. The detection is based on a digital thermoelectrically cooled CCD camera, which enables us to quantitatively and dynamically determine GFP fluorescence (i.e., expression) levels in the cytoplasm over time. When specific dyes are used to indicate subcellular organelles, the DVDM system also allows detection of multiple, different-colored fluorescence signals simultaneously from cells with high sensitivity together with their morphology in three dimensions without damaging cells (9). The figure in Supporting Information is an example of this application. With this system, it is possible to investigate at a specific time point which subcellular organelles are involved in the lipofection process and critical events, such as intracellular trafficking of plasmid DNA, interaction, or synchronization of multiple subcellular organelles.

One of the critical features of cationic lipid, polymers, lipid nanoparticles, lipoplexes, or polyplexes is the zeta potential, which reflects charge force for nucleotide binding. Both size distribution and zeta potential may change after the formation of complexes with plasmid DNA. These two are important parameters of polyplex stability, and are even more critical when polyplexes are used for *in vivo* gene transfer. When forming polyplexes, the charge ratio will be a key factor affecting both zeta potential and transfection efficiency (27). A high zeta potential often benefits *in vitro* transfection, whereas neutral or negative zeta potential of lipoplexes or polyplexes may have less serum reactivity and is beneficial for

complex stability in the bloodstream (27, 28). When similar transfection efficiency is reached, a lower charge ratio (positive charge from cationic lipid over negative charge in DNA) indicates that less cationic lipid is needed for maximal plasmid DNA binding, which indicates the carrying capacity of specific lipids. We have previously shown that our PLNP formulation exhibited similar transfection efficiency when the charge ratio was changed from 1:3 to 1:5, indicating higher DNA binding and carrying capacity of this formulation (6). In the present study, we found that the zeta potential was reduced to be neutral or even negative when the charge ratio was decreased to a range from 1.25 to 1, and the data indicate that this charge ratio is beneficial for *in vivo* delivery through intravenous administration because it may have less reactivity to negatively charged serum proteins. This is a key issue that is under-addressed in the field of lipofection. The net positive charge of polyplexes or lipoplexes is the principal reason for the formation of large aggregates after intravenous administration of lipoplexes or polyplexes and may affect tissue distribution and gene transfer efficacy in specific organs, such as livers when nonviral lipid nanoparticles are used as gene transfer vectors (29). The microscopic morphology of PLNP and polyplexes, as shown in Figure 7, further confirmed the stability after complexation with plasmid DNA, and there is a striking contrast to the formation of large aggregates of lipofectamine-derived lipoplexes. Therefore, our PLNP are useful for both *in vitro* and *in vivo* gene transfer as demonstrated in our previous studies and may also be useful in delivering siRNA, similar to other cationic lipid nanoparticles (30).

In summary, the employment of novel state-of-the-art technologies in the study of lipofection represents the level of physicochemical and biological characterization that is needed to best understand the key elements involved in the lipofection process. In the present study, we have described a refined method of PCL synthesis on a multigram scale. The data demonstrate that the morphology of PLNP derived from PCL did not change significantly after interaction with plasmid DNA, which is in striking contrast to the formation of large aggregates when using lipofectamine. The large DNA carrying capacity allows PLNP to be saturated with negatively charged plasmid DNA, and the negative zeta potential of PLNP-derived polyplexes is beneficial for *in vivo* stability. The Raman spectral signatures of PCL, PLNP, and polyplexes reflect the polymeric nature of PLNP and the close interaction of PLNP with plasmid DNA. These data are in concordance with the good stability observed for PLNP in the bloodstream and the higher transfection efficiency *in vivo* compared to other formulations of lipid nanoparticles.

Acknowledgments

We thank Mr. Souvik Biswas for his assistance in preparing samples for analysis. C.W.D. is grateful for the award of an R. Bryan Miller Fellowship from the UCD Department of Chemistry during the course of this study. This work was supported by grants from the NIH (DK069939) and the UCD Medical Center (Technology Transfer Grant to J.W.), from the National Science Foundation (to T.R.H.). The Center for Biophotonics, an NSF Science and Technology Center, is managed by the University of California, Davis, under Cooperative Agreement No. PHY 0120999. Part of the data was presented in the 11th Annual meeting of the American Society for Gene Therapy (ASGT), May 28–June 1, 2008, Boston, MA. Mr. Maung Nyunt received a travel award from the ASGT for the presentation.

LITERATURE CITED

1. Li SD, Huang L. Gene therapy progress and prospects: non-viral gene therapy by systemic delivery. Gene Ther. 2006; 13:1313–1319. [PubMed: 16953249]
2. Liu L, Zern MA, Lizarzaburu ME, Nantz MH, Wu J. Poly(cationic lipid)-mediated in vivo gene delivery to mouse liver. Gene Ther. 2003; 10:180–187. [PubMed: 12571647]
3. He SQ, Zhang YH, Venugopal SK, Dicus CW, Perez RV, Ramsamooj R, Nantz MH, Zern MA, Wu J. Delivery of antioxidative enzyme genes protects against ischemia/reperfusion-induced liver injury in mice. Liver Transpl. 2006; 12:1869–1879. [PubMed: 17133584]

4. Wu J, Liu L, Yen RD, Catana A, Nantz MH, Zern MA. Liposome-mediated extracellular superoxide dismutase gene delivery protects against acute liver injury in mice. Hepatology. 2004; 40:195–204. [PubMed: 15239103]
5. Luedde T, Trautwein C. The role of oxidative stress and antioxidant treatment in liver surgery and transplantation. Liver Transpl. 2006; 12:1733–1735. [PubMed: 17133562]
6. Wu J, Lizarzaburu ME, Kurth MJ, Liu L, Wege H, Zern MA, Nantz MH. Cationic lipid polymerization as a novel approach for constructing new DNA delivery agents. Bioconjugate Chem. 2001; 12:251–257.
7. Estrada R, Yappert MC. Alternative approaches for the detection of various phospholipid classes by matrix-assisted laser desorption/ionization time-of-flight mass spectrometry. J Mass Spectrom. 2004; 39:412–422. [PubMed: 15103655]
8. Chan JW, Motton D, Rutledge JC, Keim NL, Huser T. Raman spectroscopic analysis of biochemical changes in individual triglyceride-rich lipoproteins in the pre-and postprandial state. Anal. Chem. 2005; 77:5870–5876. [PubMed: 16159116]
9. Falk MM. Connexin-specific distribution within gap junctions revealed in living cells. J. Cell Sci. 2000; 113:4109–4120. (Pt 22). [PubMed: 11058097]
10. Wu J, Liu P, Zhu JL, Maddukuri S, Zern MA. Increased liver uptake of liposomes and improved targeting efficacy by labeling with asialofetuin in rodents. Hepatology. 1998; 27:772–778. [PubMed: 9500706]
11. Aberle AM, Bennett MJ, Malone RW, Nantz MH. The counterion influence on cationic lipid-mediated transfection of plasmid DNA. Biochim. Biophys. Acta. 1996; 1299:281–283. [PubMed: 8597581]
12. Madruga EL, San Roman J, Benedi P. High conversion polymerization of methyl methacrylate in the presence of n-dodecylmercaptan. J. Appl. Polym. Sci. 1990; 41:1133–1140.
13. Dorn K, Klingbiel RT, Specht DP, Tyminski PN, Ringsdorf H, O'Brien DF. Permeability characteristics of polymeric bilayer membranes from methacryloyl and butadiene lipids. J. Am. Chem. Soc. 1984; 106:1627–1633.
14. Chan J, Fore S, Wachsmann-Hogiu S, Huser T. Raman spectroscopy and microscopy of individual cells and cellular components. Laser Photon Rev. 2008; 2:325–334.
15. Manoharan R, Wang Y, Feld MS. Histochemical analysis of biological tissues using Raman spectroscopy. Spectrochim. Acta, Part A. 1996; 52:215–249.
16. Huser T, Orme C, Hollars C, Corzett M, Balhorn R. Raman spectroscopy of DNA packaging in individual human sperm cells distinguishes normal from abnormal cells. J. Biophotonics. 2009; 2:322–332. [PubMed: 19373853]
17. Serban D, Benevides JM, Thomas GJ. DNA secondary structure and Raman markers of supercoiling in Escherichia coli plasmid pUC19. Biochemistry. 2002; 41:847–853. [PubMed: 11790106]
18. Pelisek J, Gaedtke L, DeRouchey J, Walker GF, Nikol S, Wagner E. Optimized lipopolyplex formulations for gene transfer to human colon carcinoma cells under in vitro conditions. J. Gene Med. 2006; 8:186–197. [PubMed: 16245365]
19. Almofti MR, Harashima H, Shinohara Y, Almofti A, Baba Y, Kiwada H. Cationic liposome-mediated gene delivery: biophysical study and mechanism of internalization. Arch. Biochem. Biophys. 2003; 410:246–253. [PubMed: 12573284]
20. Elfinger M, Uzgun S, Rudolph C. Nanocarriers for gene delivery - polymer structure, targeting ligands and controlled-release devices. Curr. Nanosci. 2008; 4:322–353.
21. Ambegia E, Ansell S, Cullis P, Heyes J, Palmer L, MacLachlan I. Stabilized plasmid-lipid particles containing PEG-diacylglycerols exhibit extended circulation lifetimes and tumor selective gene expression. Biochim. Biophys. Acta. 2005; 1669:155–163. [PubMed: 15893518]
22. Braun CS, Jas GS, Choosakoonkriang S, Koe GS, Smith JG, Middaugh CR. The structure of DNA within cationic lipid/DNA complexes. Biophys. J. 2003; 84:1114–1123. [PubMed: 12547792]
23. Wachsmann-Hogiu S, Weeks T, Huser T. Chemical analysis in vivo and in vitro by Raman spectroscopy-from single cells to humans. Curr. Opin. Biotechnol. 2009; 20:1–11. [PubMed: 19394811]

24. Chan J, Fore S, Wachsmann-Hogiu S, Huser T. Raman spectroscopy and microscopy of individual cells and cellular components. Laser Photon Rev. 2008; 2:325–334.

25. Chan JW, Motton D, Rutledge JC, Keim NL, Huser T. Raman spectroscopic analysis of biochemical changes in individual triglyceride-rich lipoproteins in the pre-and postprandial state. Anal. Chem. 2005; 77:5870–5876. [PubMed: 16159116]

26. Lang I, Scholz M, Peters R. Molecular mobility and nucleocytoplasmic flux in hepatoma cells. J. Cell Biol. 1986; 102:1183–1190. [PubMed: 2420804]

27. Eliyahu H, Joseph A, Schillemans JP, Azzam T, Domb AJ, Barenholz Y. Characterization and in vivo performance of dextran-spermine polyplexes and DOTAP/cholesterol lipoplexes administered locally and systemically. Biomaterials. 2007; 28:2339–2349. [PubMed: 17298842]

28. Fumoto S, Kawakami S, Shigeta K, Higuchi Y, Yamashita F, Hashida M. Interaction with blood components plays a crucial role in asialoglycoprotein receptor-mediated in vivo gene transfer by galactosylated lipoplex. J. Pharmacol. Exp. Ther. 2005; 315:484–493. [PubMed: 16033911]

29. Wu J, Nantz MH, Zern MA. Targeting hepatocytes for drug and gene delivery: emerging novel approaches and applications. Front. Biosci. 2002; 7:d717–d725. [PubMed: 11861224]

30. Kim HR, Kim IK, Bae KH, Lee SH, Lee Y, Park TG. Cationic solid lipid nanoparticles reconstituted from low density lipoprotein components for delivery of siRNA. Mol. Pharm. 2008; 5:622–631. [PubMed: 18461969]

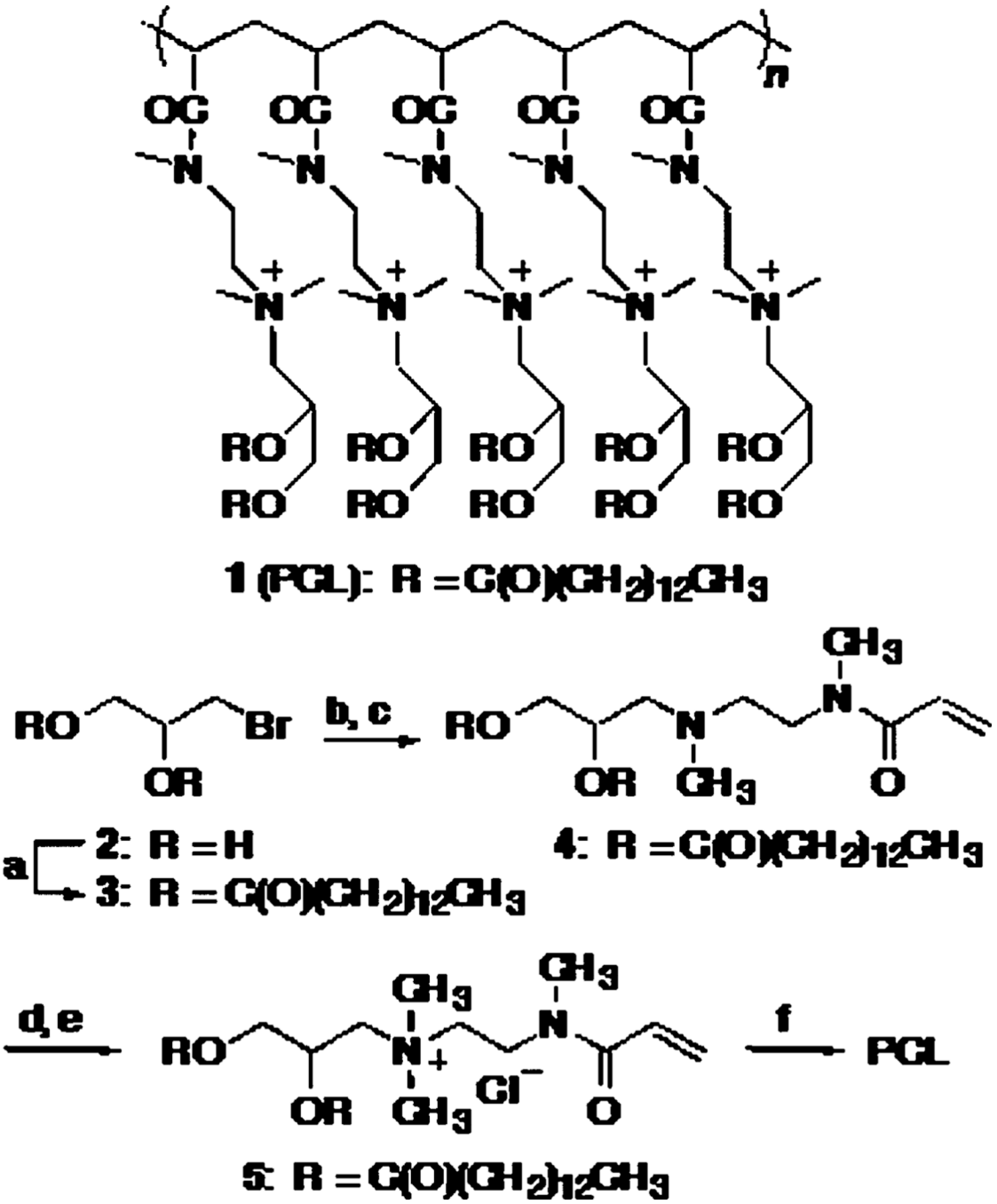

Figure 1.

PCL synthetic route: (a) myristoyl chloride (2.5 equiv), Et_3N, cat. DMAP, CH_2Cl_2, 0 °C to rt, 3 h, 92%; (b) *N*,*N*′-dimethylethylenediamine (8 equiv), DMF, 70 °C, 45 min; (c) acryloyl chloride (1.5 equiv), Et_3N, CH_2Cl_2, 0 °C - rt, 2 h, 32% (2 steps); (d) CH_3I, rt, 18 h; (e) DOWEX 1 × 8–400, CH_2Cl_2/MeOH (9:1), 92% (2 steps); (f) *n*-dodecyl mercaptan (0.34 equiv), AAPH (0.1 equiv), H_2O, 80 °C, 15 h, 97%.

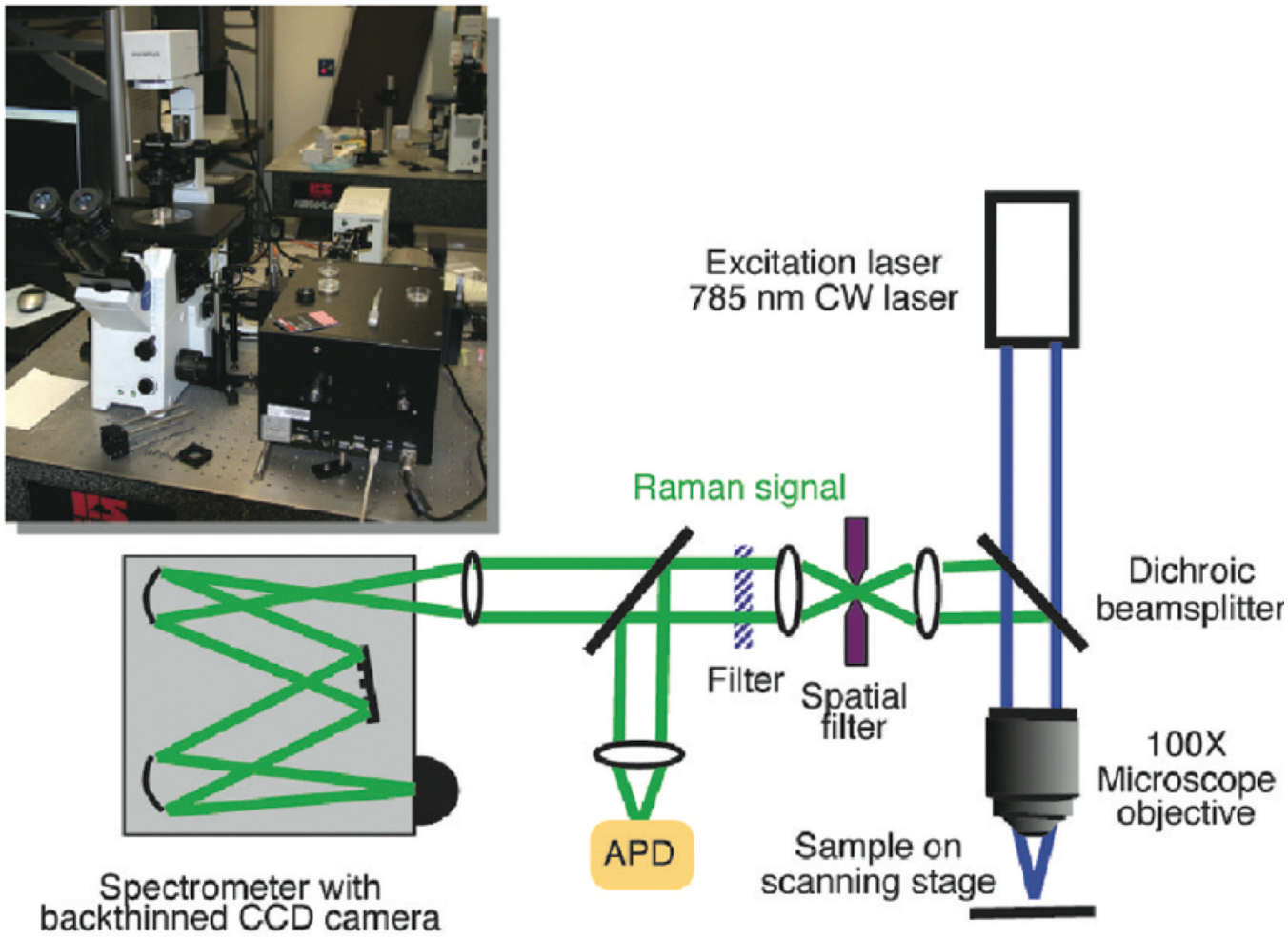

Figure 2.
Schematic diagram of the Raman system combining a microscope, confocal detection system, and various laser sources. See the Methods and Materials part for details.

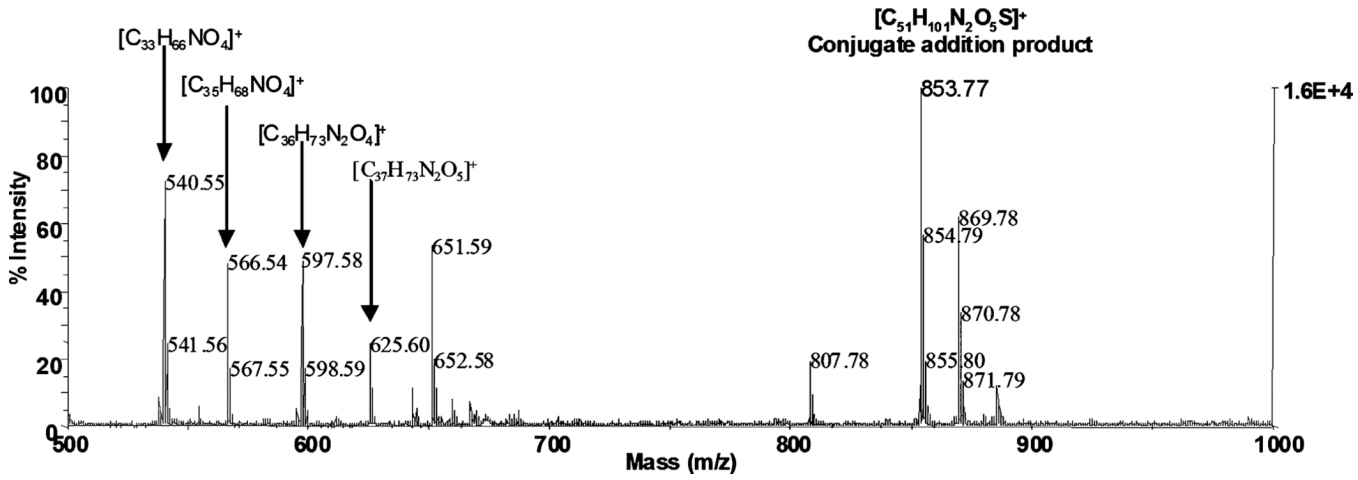

Figure 3.

Mass spectral analysis of polycationic lipids. MALDI mass spectrum of PCL was obtained with the use of *para*-nitroaniline as the matrix. Mass spectra were recorded on a Voyager Biospectrometry DE workstation in both positive and negative modes. Strong signals with maximal intensity at *m/z* = 651.6 were observed in positive-ion spectra, indicating the product of polymerized cationic lipids (PCL).

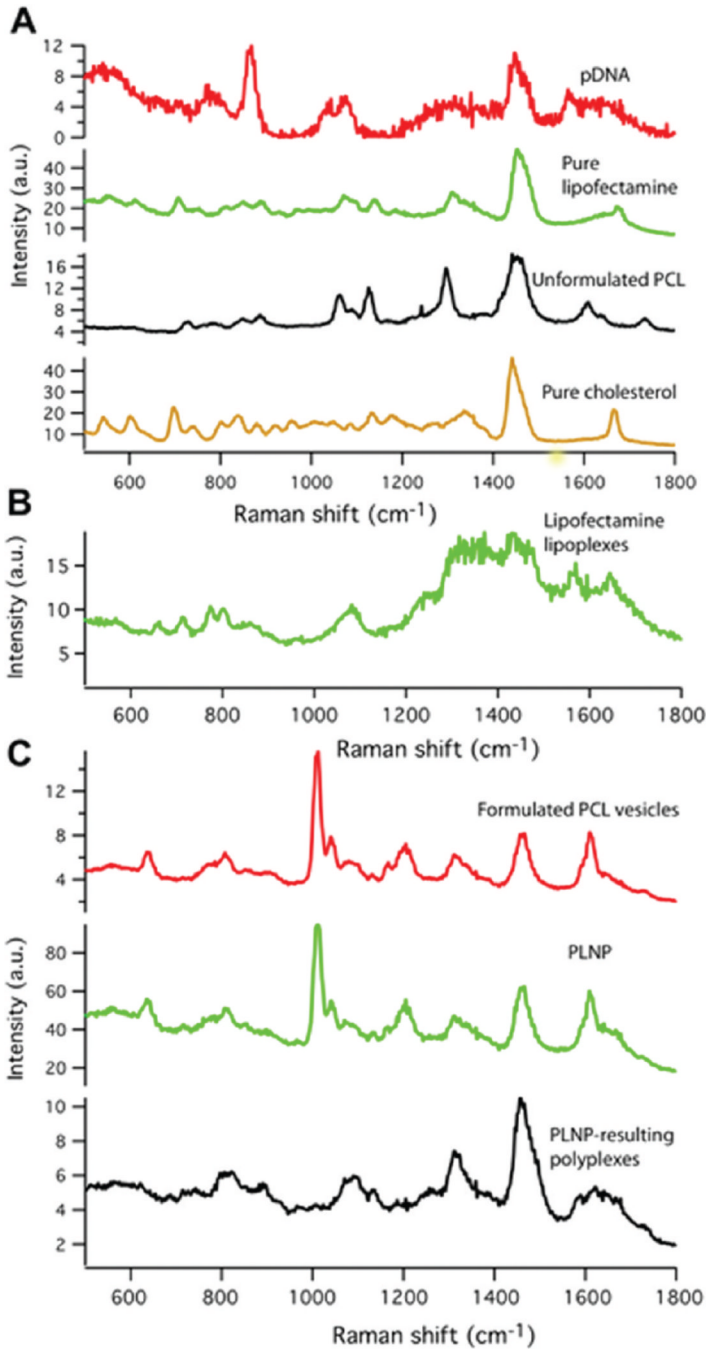

Figure 4.

Representative Raman spectrum of pure compounds, nanoparticles, and lipoplexes or polyplexes. (A) Plasmid DNA (red), pure lipofectamine (green), unformulated PCL (black), and pure cholesterol (orange). (B) Lipofectamine-derived lipoplexes (green) in 30s signal integration time. (C) PCL vesicles (red), PLNP (green), and PLNP-derived polyplexes (black). The Raman spectrum was obtained in a Laser-Tweezers Raman microspectroscopy system, and representative spectrum is shown from each condition.

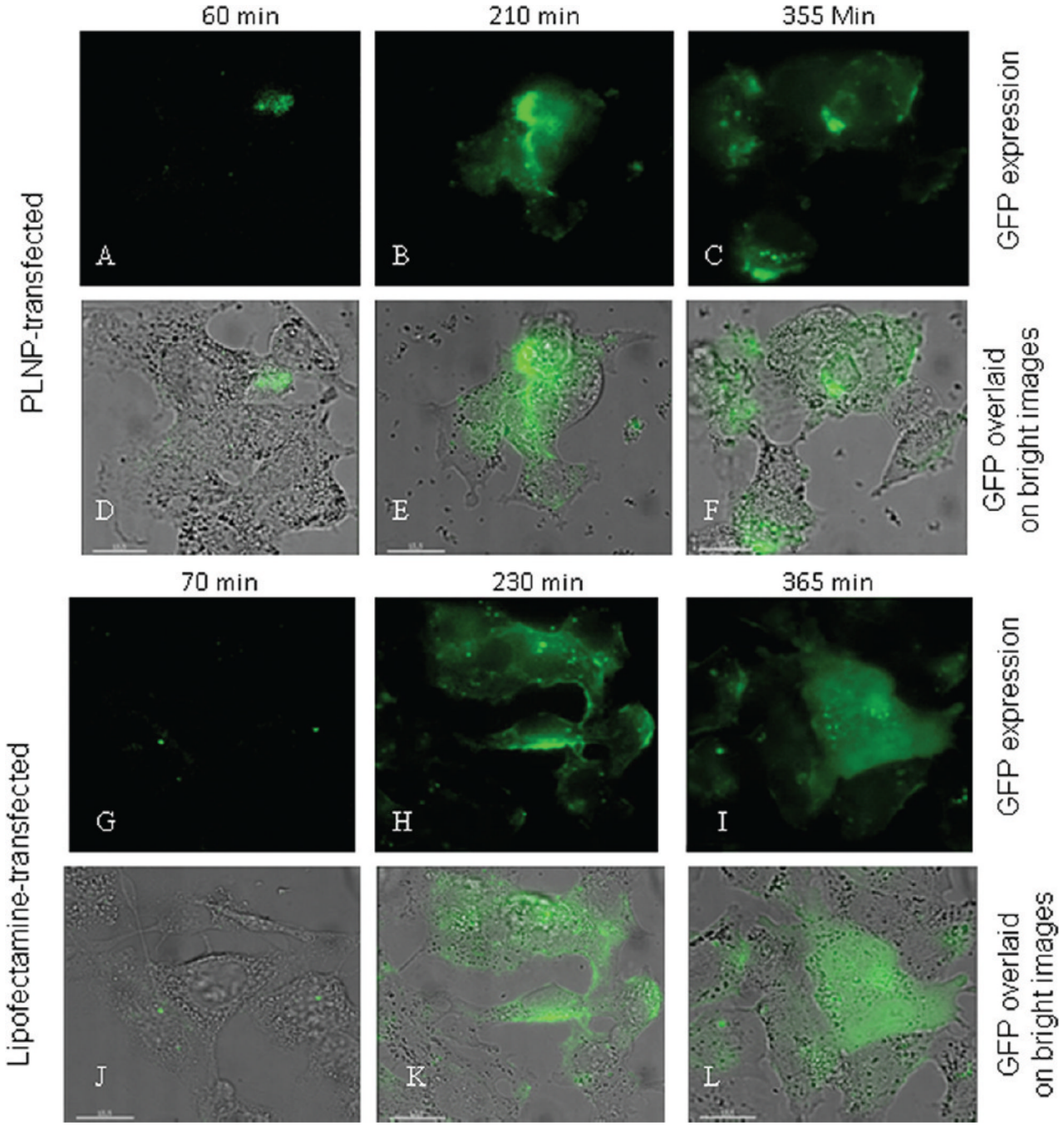

Figure 5.

Representative vertical section images of automated fluorescence deconvolution microscopy examination of GFP expression in Hep G2 cells. After transfection, the culture well was mounted in the temperature-controlled platform. Image capture is achieved with a fast, high-resolution, high quantum efficiency, thermoelectrically cooled CCD camera at various time points as indicated. A, B, C and G, H, I representative images are selected from a stack of vertical section images of individual cells at indicated time points. C, D, E, and J, K, L are the overlaid images of A, B, C and G, H, I with their bright field images.

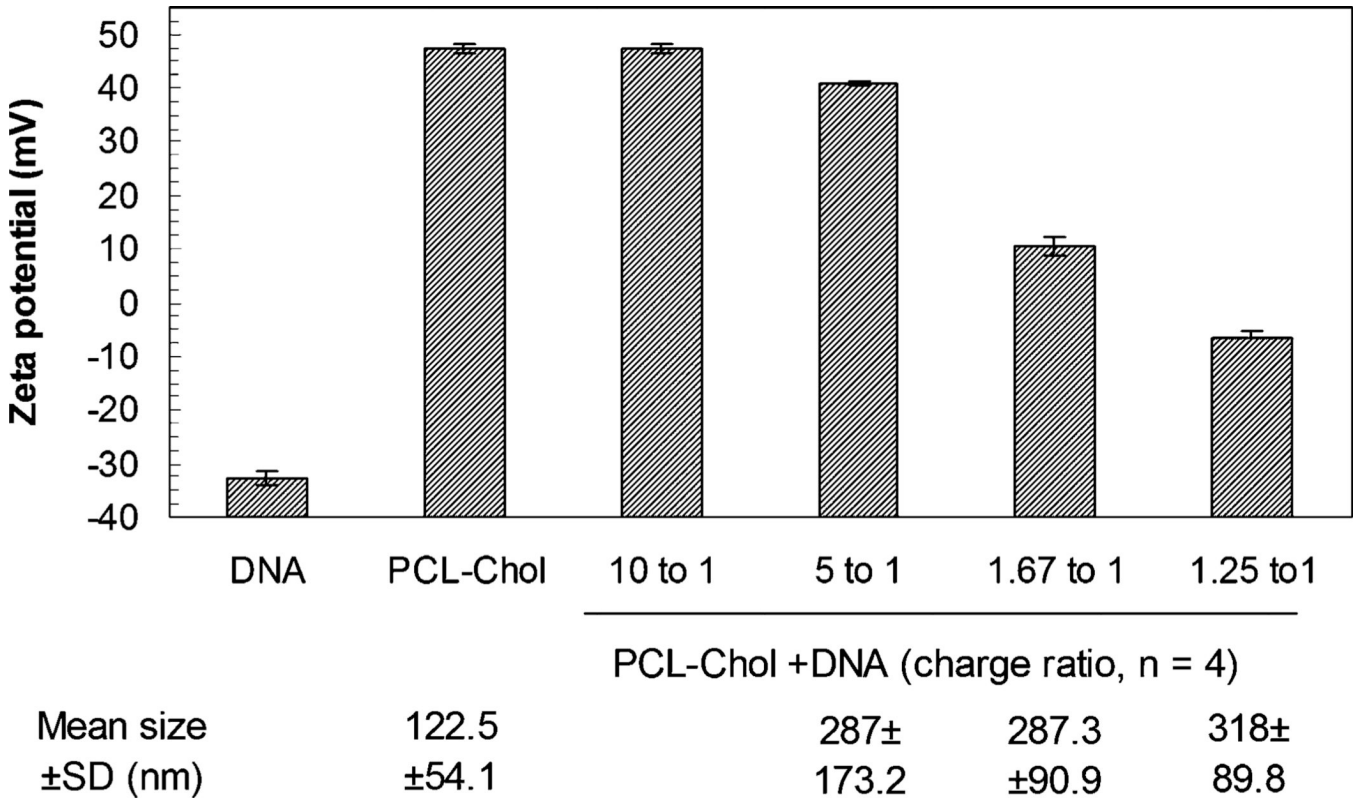

Figure 6.

Zeta potential and size changes of PLNP formulation (PCL-Chol). The zeta potential and size were measured by a zeta potential/particle sizer at the charge ratios used for both *in vitro* and *in vivo* experiments ($n = 3$). It is found that the zeta potential was reduced to be neutral or even negative when the charge ratio was decreased to a range from 1.25 to 1, and that lipoplex size increased, but stayed within the 200–400 nm range.

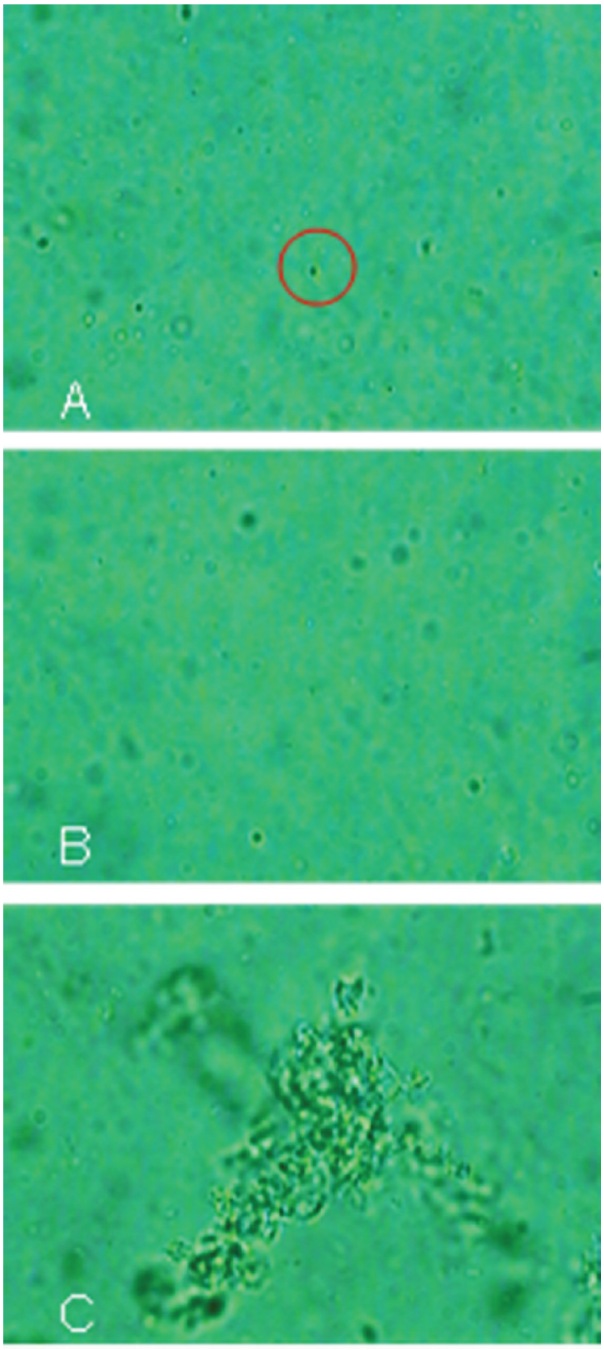

Figure 7.
Visualization of lipid vesicles under a light microscope. (A) A PLNP vesicle was visualized under the microscope used for Raman spectromicroscopy analysis (600×), and it is marked with a circle. (B) Polyplexes derived from PLNP and plasmid DNA. (C) Lipoplexes derived from lipofectamine with plasmid DNA. The PLNP morphology of these particles did not change after complexation with plasmid DNA; however, lipofectamine formed large aggregates in the presence of plasmid DNA.